

NACA TN No. 1894

8331



NATIONAL ADVISORY COMMITTEE FOR AERONAUTICS

TECHNICAL NOTE

No. 1894

BOUNDARY-LAYER AND STALLING CHARACTERISTICS OF THE
NACA 63-009 AIRFOIL SECTION

By Donald E. Gault

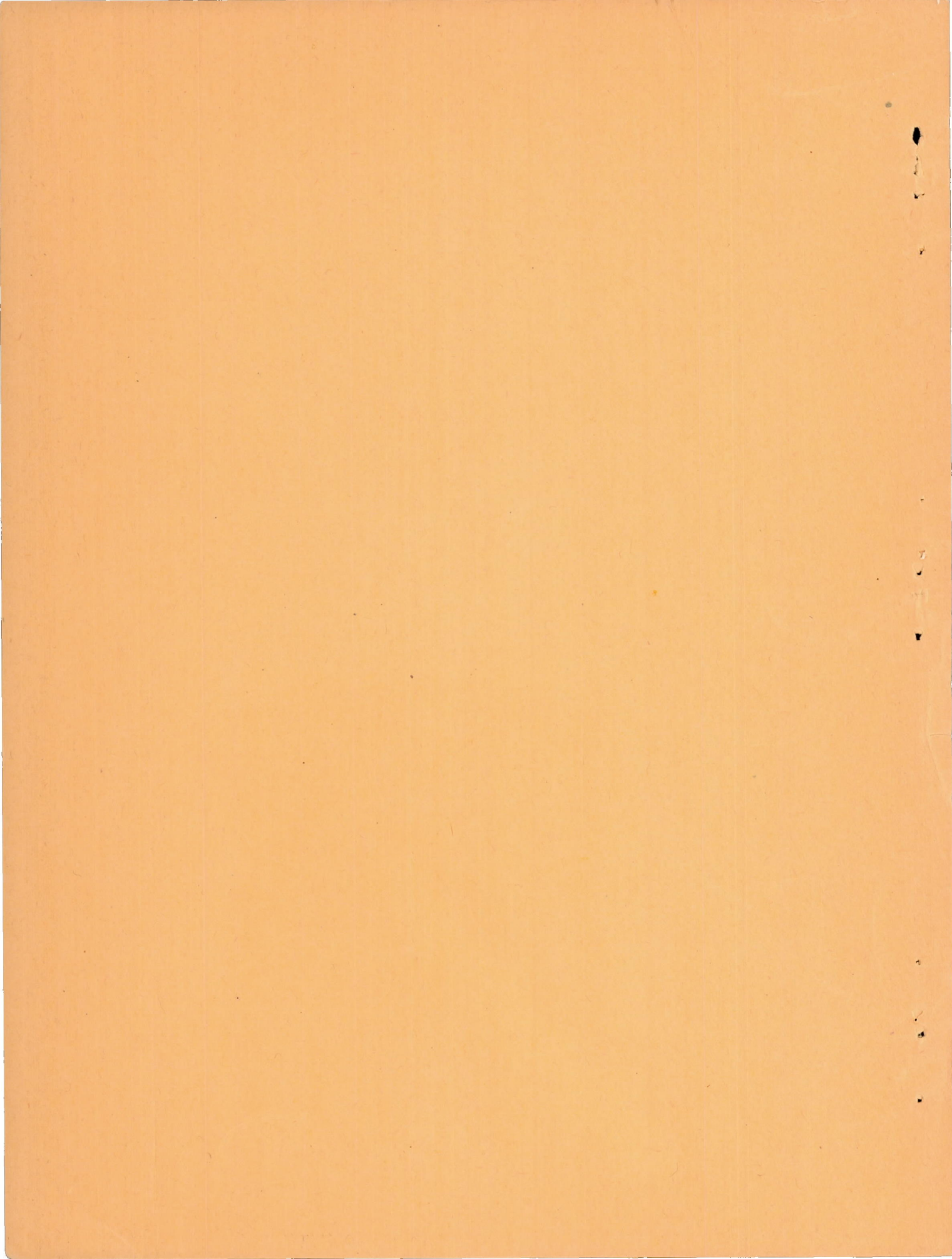
Ames Aeronautical Laboratory
Moffett Field, Calif.



Washington
June 1949

AFMDC
TECHNICAL LIBRARY
AFL 2811

319.98/41





NATIONAL ADVISORY COMMITTEE FOR AERONAUTICS

TECHNICAL NOTE NO. 1894

BOUNDARY-LAYER AND STALLING CHARACTERISTICS OF THE

NACA 63-009 AIRFOIL SECTION

By Donald E. Gault

SUMMARY

A wind-tunnel investigation was conducted to determine the boundary-layer and stalling characteristics of the NACA 63-009 airfoil section. Pressure distributions, tuft studies, and boundary-layer measurements were obtained for a Reynolds number of 5.8 million.

It was found that a localized region of separated flow developed on the upper surface of the airfoil near the leading edge. This region or "bubble" of separated flow first appeared, to a measurable extent, at a section lift coefficient of approximately 0.48. The flow separated while the boundary layer was laminar and, after the occurrence of transition, re-established itself on the surface as a turbulent boundary layer. The bubble of separated flow persisted throughout the upper lift-coefficient range until the airfoil stalled abruptly at a maximum section lift coefficient of 1.06. It was indicated that the stall was caused by the failure of the separated boundary-layer flow to reattach to the airfoil surface. Included is a discussion of the flow about the airfoil in the stalled condition.

INTRODUCTION

A previous investigation was concerned with extensive studies of the boundary-layer and stalling characteristics of two airfoil sections (NACA 63-018 and 63-012). The purpose of the studies was to gain a more precise understanding of stall phenomena and to obtain information which would be of assistance in applications

of boundary-layer control for increasing the maximum lift coefficients and improving the stalling characteristics of airfoil sections.¹

In order to extend this research to include the boundary-layer and stalling characteristics of a thinner airfoil, a similar investigation was made of the NACA 63-009 airfoil section and is reported herein. Particular attention was devoted to studying the boundary-layer flow near the leading edge where localized regions of separated flow were found to occur. The detailed measurements obtained are of interest in augmenting the meager experimental data (references 2 and 3) available on detached laminar boundary layers near an airfoil leading edge.

The data obtained include pressure-distribution measurements, tuft studies, and boundary-layer measurements for a Reynolds number of 5.8 million. The boundary-layer flow at the airfoil leading edge was studied both by direct measurements of the velocity profiles and by a technique of flow visualization employing a film of liquid on the surface.

This investigation was conducted in the Ames 7- by 10-foot wind tunnel No. 1.

SYMBOLS

The symbols used throughout this report are defined as follows:

- c airfoil chord, feet
- c_l section lift coefficient, determined by integration of the pressure distributions considering the normal and chord-wise components of the pressure forces.
- H boundary-layer shape parameter (δ^*/θ)
- h_0 free-stream total pressure, pounds per square foot
- h local total pressure inside the boundary layer, pounds per square foot
- p local static pressure, pounds per square foot

¹An investigation of boundary-layer control as applied to the NACA 63₁-012 airfoil section is reported in reference 1.

- q_0 free-stream dynamic pressure $\left(\frac{1}{2} \rho_0 U_0^2 \right)$, pounds per square foot
- S pressure coefficient $\left(\frac{h_0 - p}{q_0} \right)$
- U local velocity outside boundary layer, feet per second
- U_0 free-stream velocity, feet per second
- u local velocity inside boundary layer, feet per second
- x distance from airfoil leading edge measured parallel to chord line, feet
- y distance above airfoil measured normal to surface, feet
- α_0 section angle of attack
- δ total boundary-layer thickness, feet
- δ^* boundary-layer displacement thickness, feet

$$\left[\int_0^{\delta} \left(1 - \frac{u}{U} \right) dy \right]$$

- θ boundary-layer momentum thickness, feet

$$\left[\int_0^{\delta} \frac{u}{U} \left(1 - \frac{u}{U} \right) dy \right]$$

- ρ_0 free-stream mass density, slugs per cubic foot

APPARATUS AND METHOD

For this investigation a 5-foot-chord model was constructed of laminated mahogany to the coordinates of the NACA 63-009 airfoil section (table I). The model spanned the 7-foot dimension of the wind tunnel so that two-dimensional flow was approximated. Attached to the ends of the model were circular plates, 6 feet in diameter, which formed part of the tunnel floor and ceiling. To permit the measurement of the pressure distributions, flush pressure orifices (as noted in table I) were provided along the midspan of the model. A photograph of the model installed in the wind tunnel is presented in figure 1.

The lift characteristics of the airfoil section were obtained by mechanical integration of graphs of the pressure distributions uncorrected for tunnel-wall constraint.

Tuft studies were made by observing the flow patterns as indicated by short lengths of thread glued to the surface of the model. In addition, tufts spaced along wires extending outward from the surface and a single-tuft probe were used to investigate the flow above the airfoil surface in the stalled condition.

Boundary-layer velocity profiles were measured by means of small rakes fastened securely to the airfoil surface with small wood screws. Each rake consisted of one static-pressure tube and several total-pressure tubes. The smallest rake, used for boundary layers less than 0.10 inch thick, was made from 0.015-inch-outside-diameter steel tubing. The ends of the six total-pressure tubes were flattened to approximately oval shape, thus reducing the tube openings to less than 0.002 inch in the y direction. The heights of the tubes above the airfoil surface were measured to the centers of the open ends with a micrometer microscope to the nearest 0.0005 inch. When the rakes were installed on the airfoil in a region of appreciable curvature the tubes were bent to conform with the surface contour. The larger rakes were made from 0.030- and 0.040-inch-outside-diameter steel tubing; the largest contained 20 total-pressure tubes and permitted investigating boundary layers up to 10 inches in thickness. In addition, a special rake of 12 static-pressure tubes was employed to determine the static pressures above the airfoil surface. For the larger rakes, tube heights were measured with a steel scale and magnifying glass to the nearest 0.005 inch.

The boundary-layer velocity profiles were calculated using the relationship

$$\frac{u}{U} = \sqrt{\frac{h - p}{h_0 - p}}$$

where p and h are the local static and total pressure inside the boundary layer, respectively, as measured by the rake tubes. The above relationship implies the classical assumption of constant static pressure through the boundary layer and incompressible flow. For the model in the stalled condition the assumption of constant static pressure could not be justified and the velocity profiles were calculated considering the measured static pressures above the airfoil surface. Because of the high local velocities at stations

forward of 0.10 chord, the pressure differences in the preceding relationship were corrected for compressibility effects (assuming adiabatic compression); for stations behind 0.10 chord these compressibility corrections were insignificant.

To supplement the boundary-layer velocity-profile measurements in the localized region of separated flow at the leading edge of the airfoil prior to the stall, the liquid-film technique described in reference 1 was employed. This method depends on the scrubbing or shearing action of the boundary-layer flow on a thin film of liquid sprayed on the model. Measurements were made of the chordwise locations of the boundaries of the bands of liquid which remained on the surface of the model after the tunnel was stopped. There was no perceptible movement of these bands while the wind tunnel was being stopped. A dull black finish on the model facilitated these observations.

All data presented were obtained at a dynamic pressure of 40 pounds per square foot which, for the 5-foot-chord model, corresponds to a Reynolds number of 5.8 million and a Mach number of 0.167.

RESULTS AND DISCUSSION

Lift Characteristics

The stall of the NACA 63-009 airfoil section was very abrupt although the loss in lift associated with the stall was not large. This result is shown in figure 2 by the variation of the section lift coefficient with section angle of attack (uncorrected for tunnel-wall constraint) as determined by mechanical integration of graphs of the pressure distributions. The sharp peak of the lift curve typifies the sudden stall of this and other moderately thin airfoil sections. However, reference 4, which presents the lift characteristics of this airfoil section for Reynolds numbers from 3 to 25 million, shows that the lift-curve peak becomes more rounded and the sudden loss of lift at the stall no longer exists for a Reynolds number of 15 million or greater. Since a change in the stalling characteristics is reflected by a change in the boundary-layer characteristics, data obtained at a Reynolds number of 5.8 million cannot, therefore, describe the characteristics which occur at the higher Reynolds numbers. Undoubtedly, there is a lower limit of applicability also, but there is insufficient information for its determination.

It should be mentioned that flow conditions corresponding to the maximum section lift coefficient ($\alpha = 8.9^\circ$; $C_{l_{max}} = 1.06$) were not stable. Frequently, after steady flow had been maintained about the airfoil for periods of time up to several minutes, the airfoil would

stall for no apparent reason. Occasionally there was a cyclic change between the stalled and unstalled conditions although, generally, once the airfoil stalled, steady flow failed to return.

Pressure Distributions

The chordwise variations of the pressure coefficient S over the surface of the airfoil are presented in figure 3 for a range of lift coefficients including the stalled condition. The values of the pressure coefficient are the observed values measured at a Mach number of 0.167 and have not been corrected to zero Mach number. No corrections for tunnel-wall constraint were applied since the corrected distributions would not depict the actual pressures which acted on the boundary layer.

The pressure distributions for the airfoil prior to the stall are normal in appearance and graphically illustrate the high pressure peaks which develop behind the leading edge of thin airfoils at moderate values of the lift coefficient. The stall occurred at an angle of attack of 9.0° and was accompanied by a redistribution of the pressures (fig. 3(b)). The abrupt change in the flow which accompanied the stall was characterized by the complete collapse of the leading-edge pressure peak and the substitution of an approximately constant-pressure region extending to 0.10 chord. Although the pressures did not recover to free-stream static pressure at the trailing edge, considerable pressure was recovered between 0.10 chord and the trailing edge. Further increases in the angle of attack increased the chordwise extent of the region of nearly constant pressure, but reduced the values of the pressure coefficients.

Tuft Studies

The tuft observations generally agreed with the lift and pressure-distribution measurements. The flow over the upper surface of the airfoil was very steady at all angles of attack prior to the stall and gave no indication of any impending change. The tufts did not indicate the existence of a localized region of separated flow near the leading edge. The transformation into the pattern characteristic of the stalled condition was seemingly instantaneous. For an angle of attack of 9° the surface tufts indicated reversed or separated flow from the leading edge to approximately 0.20 chord. Behind this region, however, no definite pattern of separated flow was observed; that is, although the flow was exceedingly rough, the tufts always indicated flow in the downstream direction. Detailed investigation of the flow over the forward portion of the airfoil with a single-tuft probe and tufts attached to wires extending outward from the surface

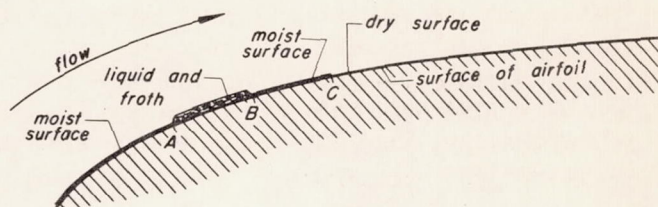
revealed that the reverse flow over the forward portion of the airfoil was part of a circulatory motion strongly suggestive of a vortex centered above the airfoil surface at about 0.05 chord. Further increases in the angle of attack beyond the onset of the stall moved the apparent vortex core downstream and increased the chordwise extent of the reverse flow.

Liquid-Film Studies

For values of the section lift coefficient greater than approximately 0.40, well-defined boundaries of a region of separated flow were observed near the leading edge during the liquid-film studies. In addition to a spanwise band of liquid and froth similar to that reported in reference 1, a second band of liquid was observed, the limits of which were defined by a dry area and the downstream edge of the liquid-and-froth band.

A schematic view of the two bands observed on the model is shown in the accompanying

diagram. From the stagnation point on the lower surface around the leading edge to A, the airfoil surface was moist; on the dark model the residual liquid gave the surface the appearance of being jet



black. Between points A and B the surface was covered with liquid, and, at lift coefficients approaching the stall, a whitish, fine-grained froth. The froth was generated downstream of B and moved rapidly upstream to form the band AB reported in reference 1. The second band BC was similar in appearance to the airfoil surface upstream of A. The downstream edge of this second band was sharply defined at C by a region which was scrubbed completely dry by the boundary-layer flow.

Measurements of the boundaries A, B, and C are presented in figure 4 for the smooth airfoil. The physical significance of the three boundaries may be explained (with knowledge of the boundary-layer-survey results which will be discussed later) in terms of the boundary-layer behavior as follows: From stagnation on the lower surface around the leading edge to A on the upper surface the

boundary layer was laminar. The liquid sprayed on the wing was moved along the surface due to the shearing action of the boundary layer to point A where separation occurred. After separation, the absence of surface shear caused the liquid to accumulate while the detached boundary layer passed on downstream. Point B, it is believed, does not represent a change in the characteristics of the boundary layer but was caused by the action of the reversed flow on the accumulated liquid. Thus, the band AB resulted from two opposing flows, causing an accumulation of liquid on the airfoil surface. At C, reattachment occurred as a transitional boundary layer and sufficient scrubbing action was present to remove all liquid from the surface.

Boundary-Layer Measurements

Turbulent boundary layer.— The boundary-layer measurements over the after portion of the unstalled airfoil are presented in figure 5 as the chordwise variations of the derived parameters, momentum thickness θ and shape parameter H . Typical boundary-layer velocity profiles from which the parameters were ascertained by mechanical integration are shown in figure 6. Only fully developed turbulent boundary layers were considered.

The boundary-layer-shape parameter H for the airfoil did not exceed a value of 1.7, a value considerably less than 2.6 which has been demonstrated to be indicative that a turbulent boundary layer has separated. On the basis of these data, it is apparent, therefore, that the stall could not have been caused by separation of the turbulent boundary layer.

Region of laminar separation.— In order to study the boundary layer at the leading edge, detailed total- and static-pressure surveys were made over the airfoil through a range of lift coefficients for which regions of separated flow had been indicated by the liquid-film method. In agreement with the liquid-film results, the region of separated flow first appeared, to a measurable extent, at an angle of attack of 4.0° ($c_l = 0.48$). These data are presented in figure 7 (together with the surface pressure distribution) as the chordwise variation in the boundary-layer velocity profiles from a point just upstream of separation to a point downstream of reattachment. The velocity profiles are plotted with their vertical axes ($u/U = 0$) on the chordwise stations at which they

were measured; the dashed portions of the profiles and cross-hatched areas represent the regions of reversed or separated flow.² The surface static pressures at stations intermediate to the flush pressure orifices in the model were ascertained from the boundary-layer surveys. Boundary-layer measurements could not be obtained for the unstable flow condition at an angle of attack of 8.9° ($C_{l_{max}} = 1.06$) since the presence of the rake was sufficient disturbance to precipitate the stall prematurely.

Examination of these data shows that the flow separation near the leading edge of the airfoil prior to the stall occurred while the boundary layer was laminar and that flow reattachment always took place with a transitional boundary layer. Transition, therefore, commenced when the boundary layer was detached from the surface. Since separated flow leaves a curved surface in a direction approximately tangent to the surface at the point of separation, transition and the ensuing expansion of turbulence were essential to re-establish the flow on the surface. In view of the absence of turbulent separation and the sudden occurrence of the stall, there can be little doubt that the stall resulted from the failure of the separated boundary-layer flow near the leading edge to reattach to the airfoil surface. Discussion of the boundary-layer flow in a region of laminar separation at an airfoil leading edge and the effects of Reynolds number on the maximum lift may be found in references 4, 5, and 6.

Increased angle of attack caused the separated region or bubble to move forward and become of shorter chordwise extent. Separation always occurred downstream of the pressure peak and, characteristic of most separated-flow regions, a short extent of constant surface pressure existed within the bubble, although pressure recovery continued downstream of the constant-pressure region before reattachment. Previous measurements of similar separated flows, reported in reference 2, are in substantial agreement with these results.

The chordwise location of the separation and reattachment points as determined by the boundary-layer surveys are compared with the liquid-film results in figure 4. This comparison is

²An investigation was conducted which revealed that in a region of reverse flow the rake static-pressure tubes indicated pressures greater than those for the rake total-pressure tubes. This same result was observed for many of the velocity profiles presented in figure 7 and aided in determining the location and extent of the separated bubble.

considerably dependent upon the manner of fairing the boundary-layer data, particularly for the points of flow reattachment at the higher angles of attack for which the shape of the distorted transitional velocity profiles is difficult to determine. The correlation between the two methods is excellent, however, considering the small chordwise extent of the region of separated flow. Since the presence of the survey rake was sufficient disturbance to cause the airfoil to stall prematurely, it seems probable that the results of the liquid-film method, having negligible interference effects, are the most reliable.

It is interesting to note the amount of pressure recovery that was obtained before laminar separation. A measure of this pressure recovery can be expressed by the ratio of the pressure coefficient at separation S_{sep} to the maximum pressure coefficient S_{max} . As determined from figure 7, the value of the ratio S_{sep}/S_{max} was about 0.89 (varying between 0.88 and 0.90). A similar ratio $(U_{sep}/U_{max})^2$ was employed in reference 7 for a theoretical study of laminar separation. By the method of reference 7 for a "single-roof pressure distribution" which approximates the experimental distribution over the airfoil leading edge, separation was predicted to occur when the pressure ratio attained a value of 0.81. For practical calculations, however, the difference between 0.81 and 0.89 would represent only a small error in locating the separation point downstream of a leading-edge pressure peak.

From the preceding discussion it will be seen that the laminar separation near the leading edge was dependent, primarily, on the amount of pressure recovery the laminar boundary layer was capable of withstanding. The magnitude of the pressure gradient ahead of separation, within the limitations of this investigation, appears to have had no effect on separation. The forward movement of the bubble with increasing angle of attack, therefore, can be explained by the corresponding movement of the pressure peak.

Similarly, the change in the chordwise extent of the bubble may be attributed to the pressures near the leading edge if the hypothesis advanced in reference 6 is assumed. According to reference 6, for regions of separated laminar flow, a constant Reynolds number may be formed which is based on the local velocity outside the boundary layer at separation and the distance between the points of separation and transition. Thus, any increase in local velocities with increased angle of attack would be counteracted by a decrease in the distance from separation to transition,

and, of course, in the chordwise extent of the bubble. This reduction in the bubble did occur, although the value of the Reynolds number as defined by the region of the separated laminar flow was inconsistent. Assuming that transition occurred just downstream of the chordwise station where the last separated laminar boundary layer was measured (fig. 7), the value of this Reynolds number for lift coefficients less than 0.8 was approximately 60,000. (A value of 50,000 was assumed in reference 6.) However, for conditions near maximum lift, the value of this Reynolds number decreased to less than 30,000. When the liquid-film results were utilized, the Reynolds number as defined by the region of the separated flow more nearly approximated a value of 60,000 for lift coefficients greater than 0.8.

Stalled condition.— The boundary-layer measurements on the airfoil in the stalled condition revealed that the static pressure above the airfoil surface was not constant through the region where viscous effects predominated (fig. 8). The pronounced static-pressure minimums above the airfoil surface near the leading edge are suggestive of the core of the vortex which was indicated by the tuft studies.

The reduced pressures at the core of this apparent vortex were transmitted downstream so that the measured static pressures were employed in calculating the velocity profiles presented in figure 9. The reverse flow near the leading edge indicated by the tuft studies is not apparent from these data, although there are discontinuities in the velocity profiles near the airfoil surface. The values of u/U greater than 1.0 may be attributable to the velocities induced by the vortex flow.

It must be emphasized, however, that the violently irregular velocities and pressures accompanying the stall could not be accurately measured in terms of mean values with the experimental technique employed. The measured values of the fluctuating pressures, therefore, cannot be expected to represent accurately any one phase of the fluctuating flow. Moreover, the existence of vortices implies velocities oblique to the survey tubes so that the static- and total-pressure measurements lose significance. However, it is thought that, due to the time-lag response of the survey-rake system, an approximation to the predominate flow condition was obtained. With the imposition of these limitations, these data for the stalled condition must be considered qualitative.

CONCLUDING REMARKS

The results of the investigation reported herein show that a localized region or bubble of separated flow appeared near the leading edge of the NACA 63-009 airfoil section after the formation of the leading-edge pressure peak and persisted throughout the upper lift-coefficient range to the stall. Separation occurred downstream of the pressure peak when the pressure had recovered to approximately 0.89 of the maximum pressure coefficient and always originated while the boundary-layer flow was of the laminar type. The separated laminar boundary layer passed on downstream with a short run at constant surface pressure and terminated when transition took place while the flow was detached from the surface. Reattachment of the flow always occurred with a transitional boundary layer. Since there was no indication of separation of the turbulent boundary layer over the rear portion of the airfoil, it is concluded that the abrupt stall resulted when the developing turbulent boundary layer near the leading edge was unable to reattach the separated flow to the surface. The stall of the airfoil section was accompanied by a complete readjustment of the flow characteristics.

Ames Aeronautical Laboratory,
National Advisory Committee for Aeronautics,
Moffett Field, Calif.

REFERENCES

1. McCullough, George B., and Gault, Donald E.: An experimental investigation of an NACA 631-012 Airfoil Section with Leading-Edge Suction Slots. NACA TN No. 1683, 1948.
2. von Doenhoff, Albert E., and Tetervin, Neal: Investigation of the Variation of Lift Coefficient with Reynolds Number at a Moderate Angle of Attack on a Low-Drag Airfoil. NACA CB, Nov. 1942.
3. Jones, Melville B.: Stalling. Jour. Royal Aero., Soc., Vol. 38, No. 285, Sept. 1934, pp. 753-770.
4. Loftin, Laurence K., Jr., and Bursnall, William J.: The Effects of Variations in Reynolds Number Between 3.0×10^6 and 25.0×10^6 upon the Aerodynamic Characteristics of a Number of NACA 6-Series Airfoil Sections. NACA TN No. 1773, 1948.

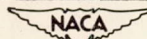
5. Jacobs, E. N., and Sherman, A.: Airfoil Section Characteristics as Affected by Variations of the Reynolds Number. NACA Rep. No. 586, 1937.
6. von Doenhoff, Albert E.: A Preliminary Investigation of Boundary-Layer Transition Along a Flat Plate with Adverse Pressure Gradient. NACA TN No. 639, 1938.
7. von Kármán, Th., and Millikan, C. B.: On the Theory of Laminar Boundary Layers Involving Separation. NACA Rep. No. 504, 1934.

TABLE I.— COORDINATES FOR THE NACA 63-009 AIRFOIL SECTION

[Stations and ordinates are in percent of the chord]

Station	Ordinate
0	0
.5	.749
.75	.906
1.25	1.151
2.5	1.582
5.0	2.196
7.5	2.655
10.0	3.024
15.0	3.591
20.0	3.997
25.0	4.275
30.0	4.442
35.0	4.500
40.0	4.447
45.0	4.296
50.0	4.056
55.0	3.739
60.0	3.358
65.0	2.928
70.0	2.458
75.0	1.966
80.0	1.471
85.0	.990
90.0	.550
95.0	.196
100.0	0

L.E. Radius = 0.631



Note: Except for station 100.0, pressure orifices were located at the above stations (upper and lower surfaces) with additional orifices at stations 0.10 and 0.25.

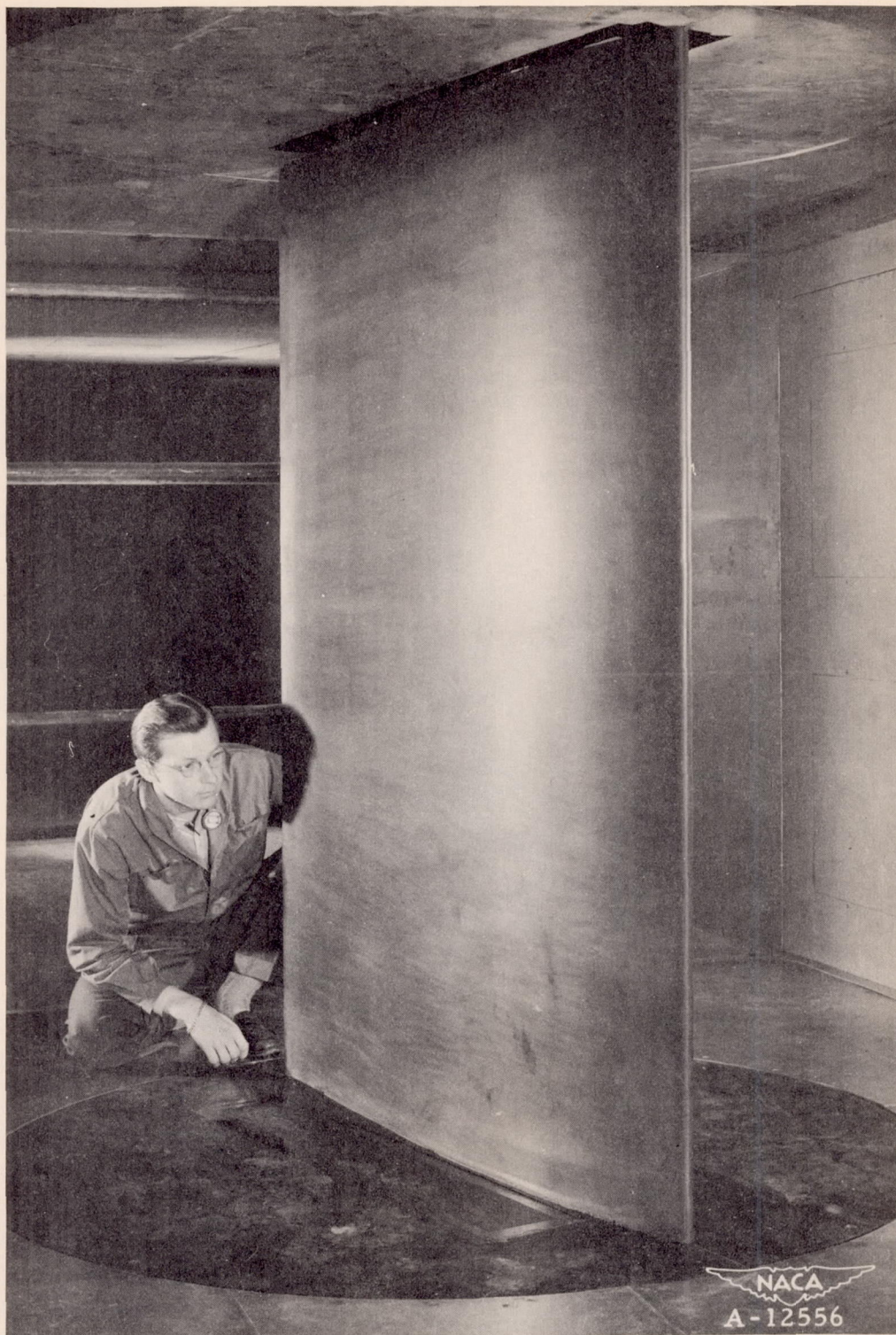


Figure 1.- The NACA 63-009 airfoil model mounted in the Ames
7- by 10-foot wind tunnel No. 1.

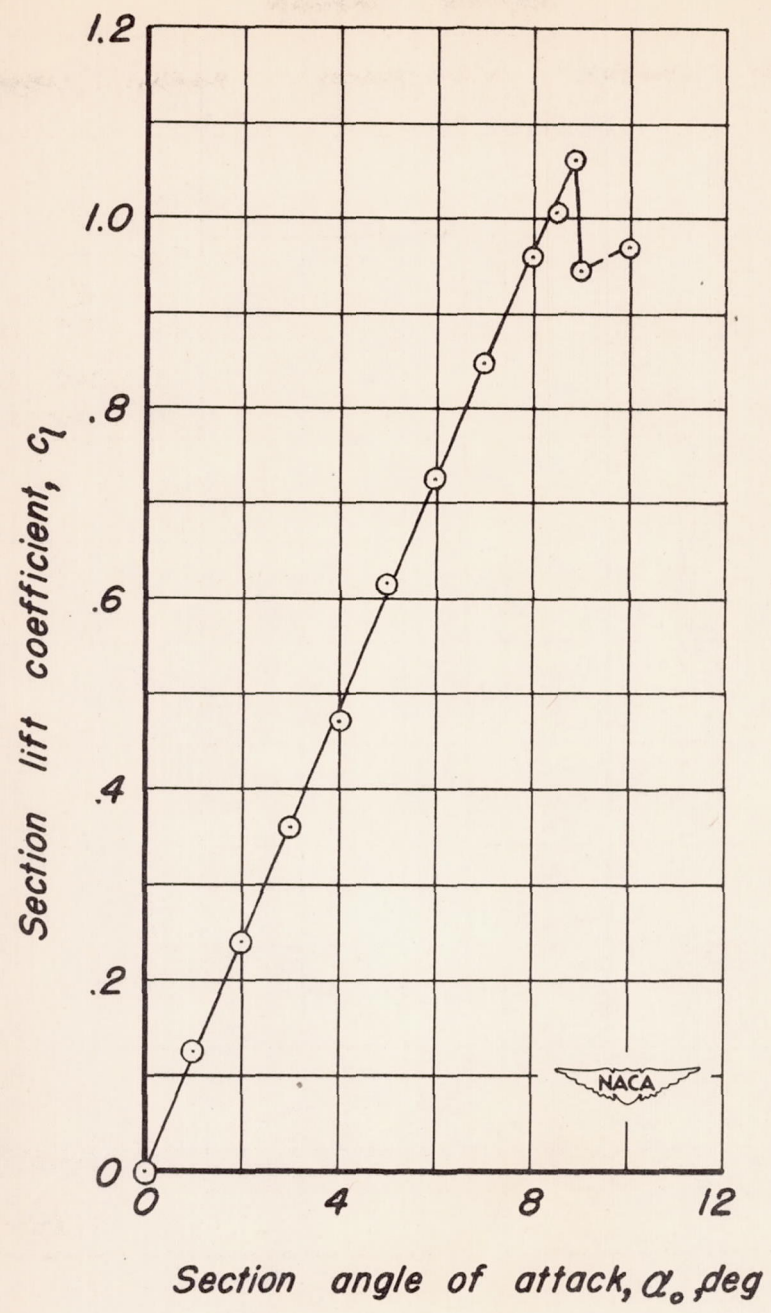


Figure 2.- Variation of the section lift coefficient with section angle of attack.

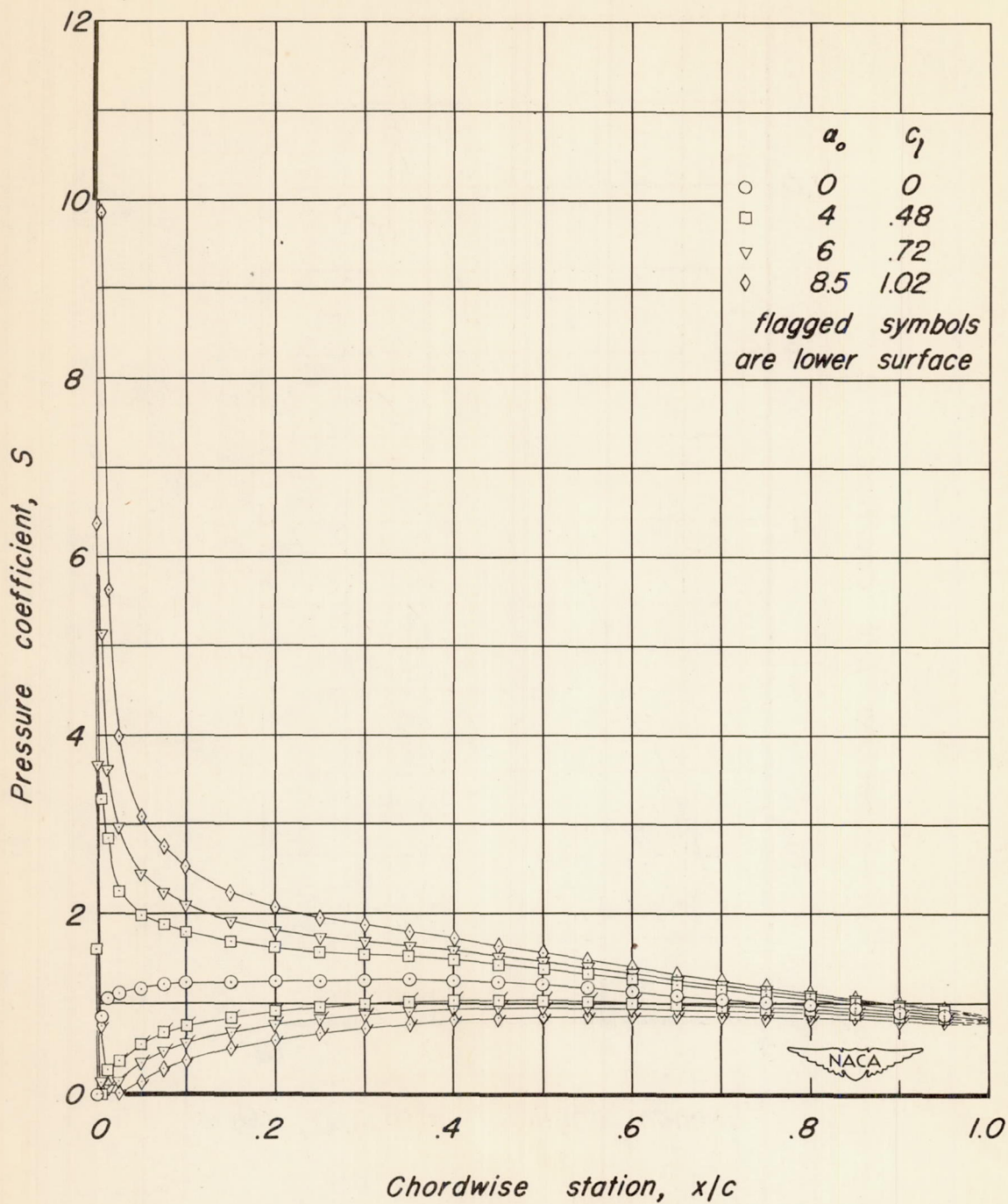
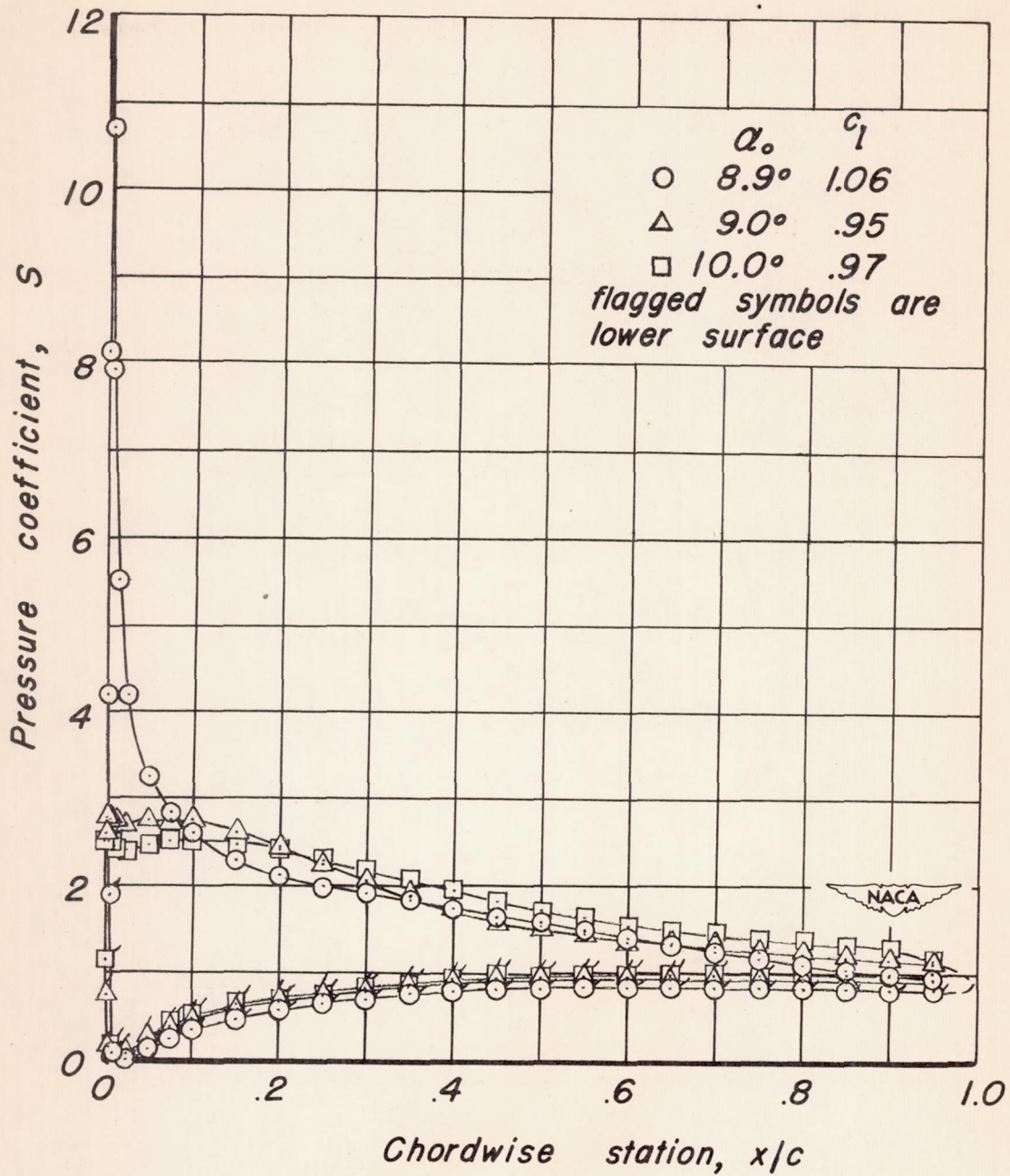
(a) $\alpha_0, 0^\circ$ to $\alpha_0, 8.5^\circ$.

Figure 3.- Pressure distributions.



(b) $\alpha_0, 8.9^\circ$ to $\alpha_0, 10.0^\circ$

Figure 3.- Concluded.

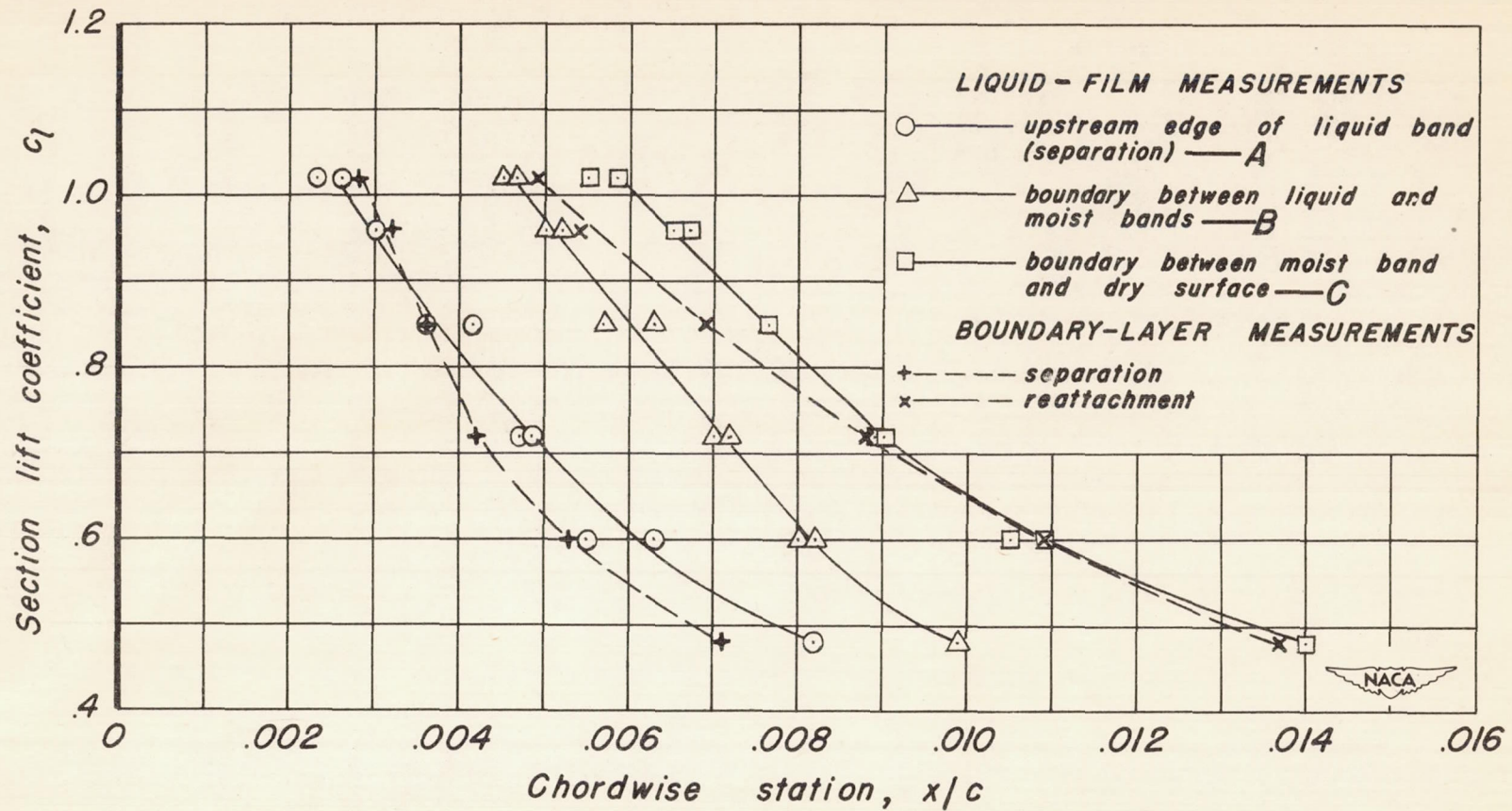


Figure 4.- Comparison between the liquid-film and boundary-layer measurements of the region of laminar separation.

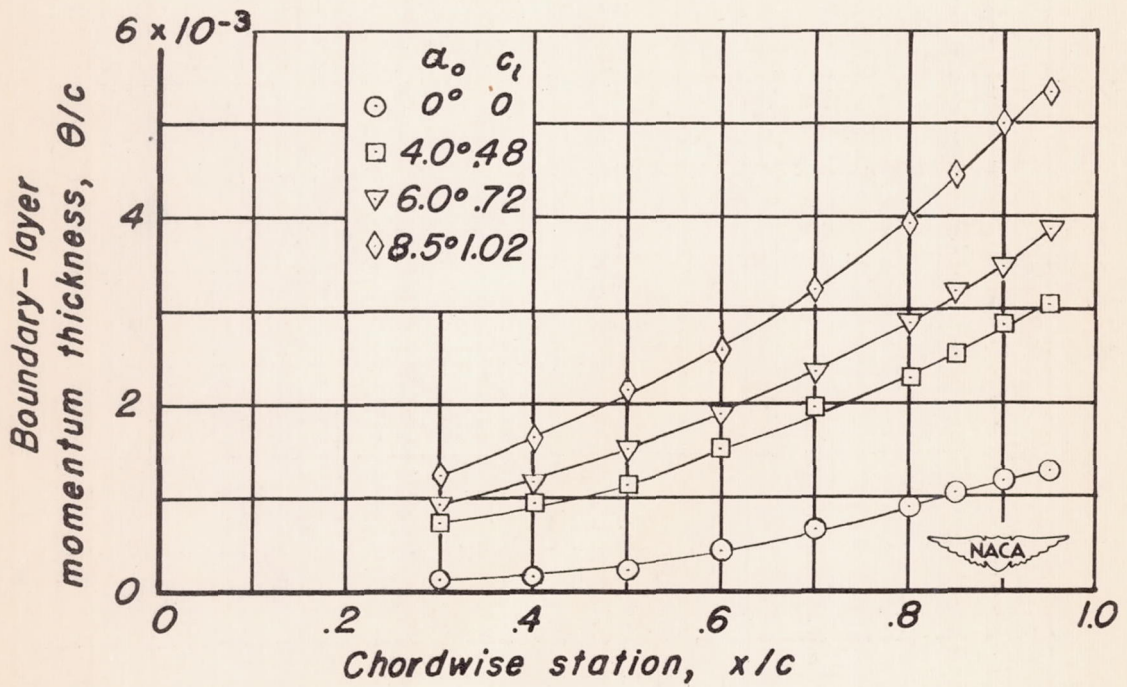
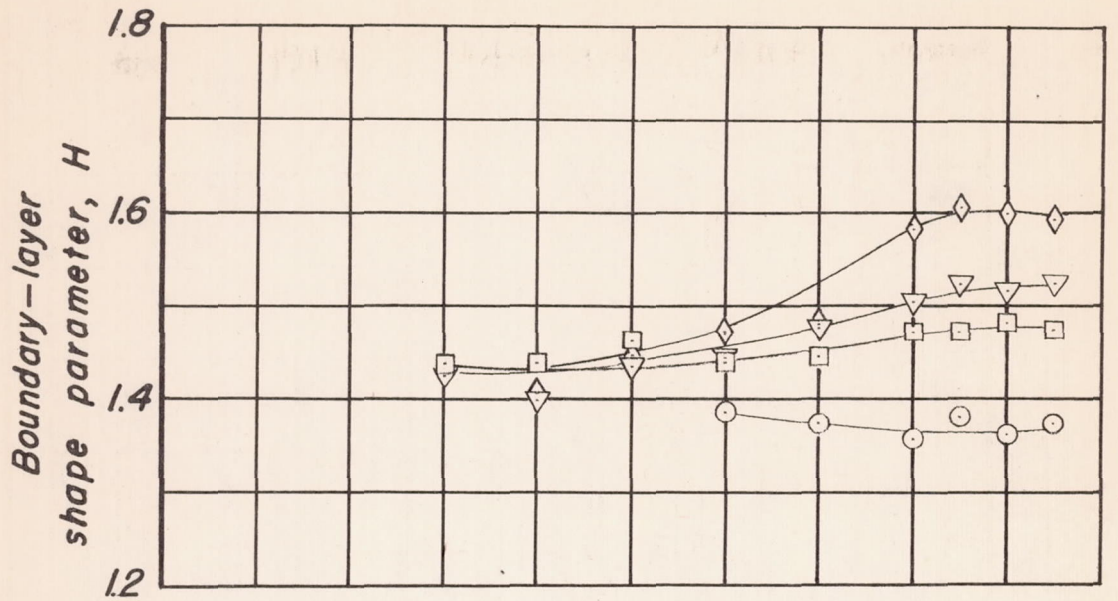


Figure 5.- Chordwise variation of the boundary-layer momentum thickness and shape parameter.

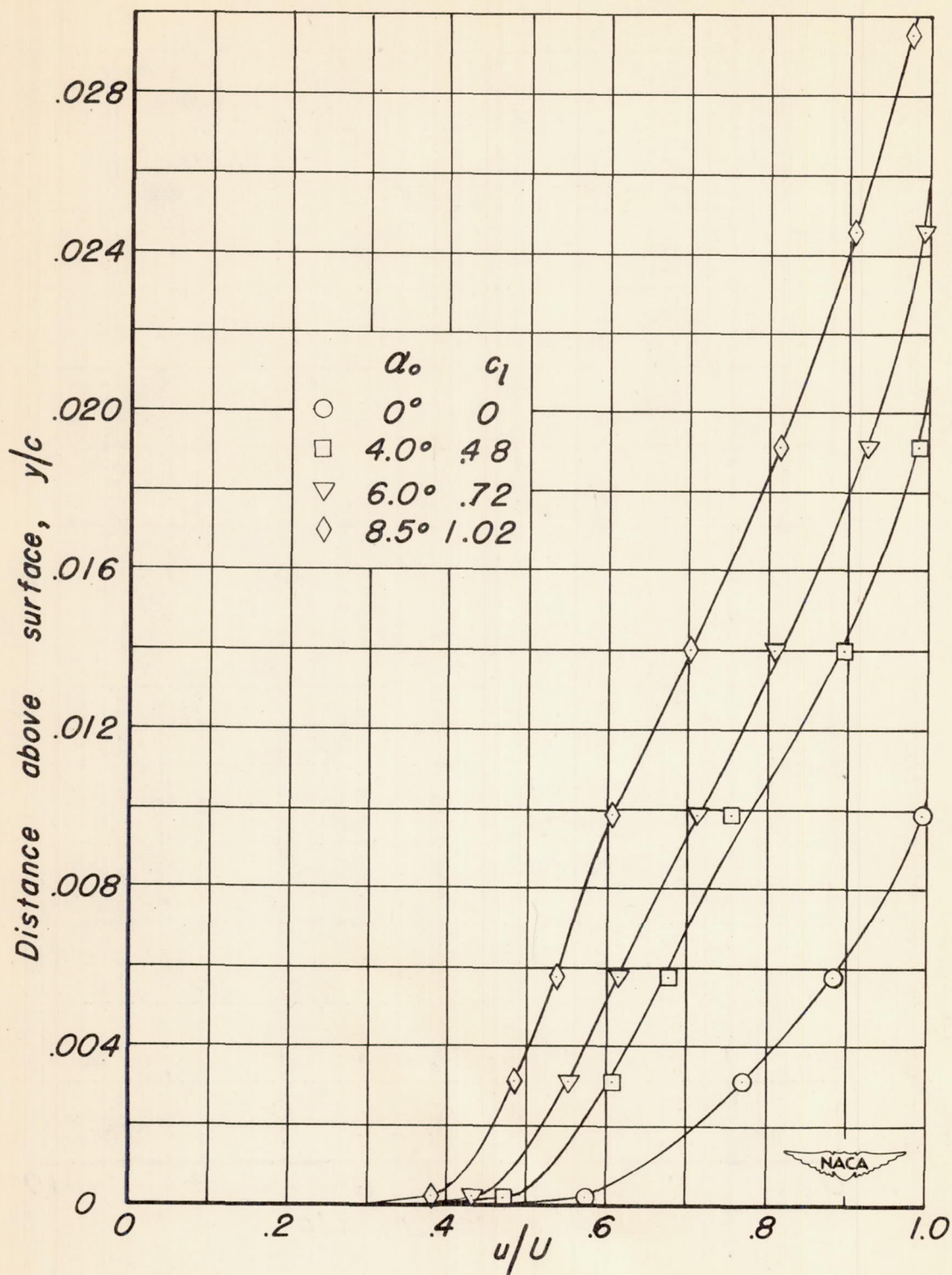
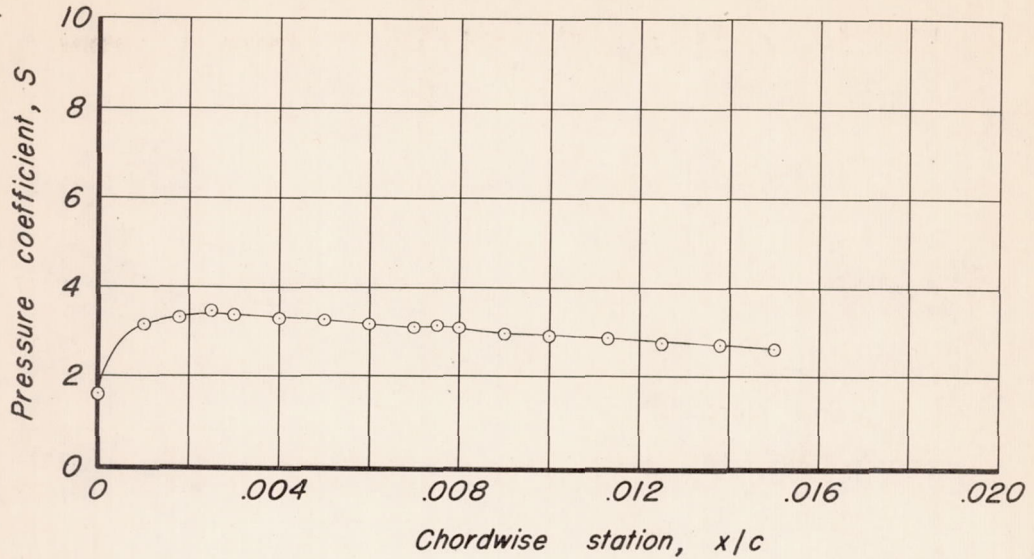
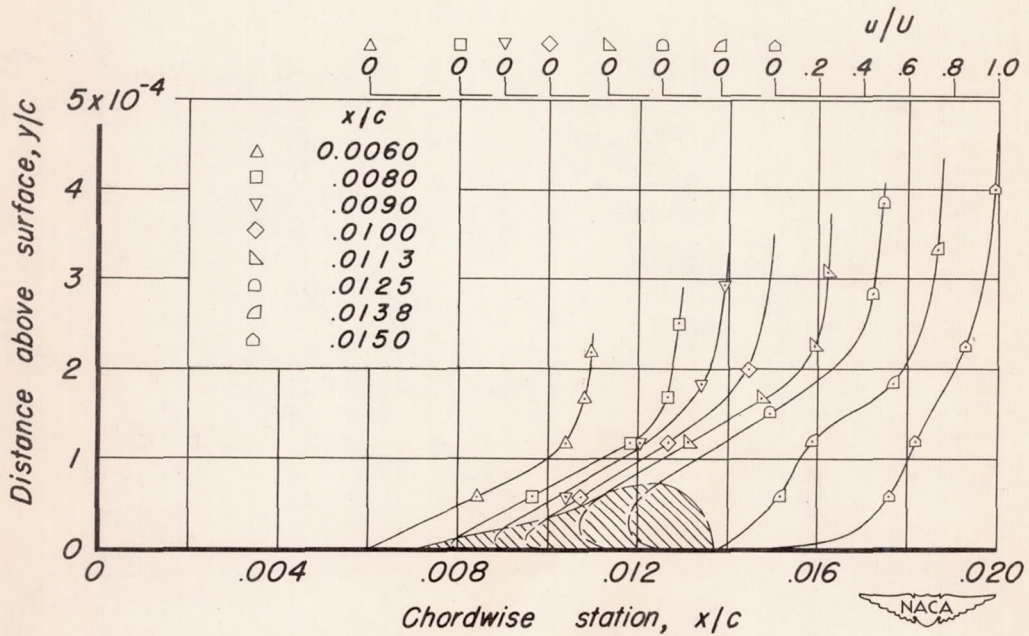


Figure 6.-Boundary-layer velocity profiles at 0.95 chord.



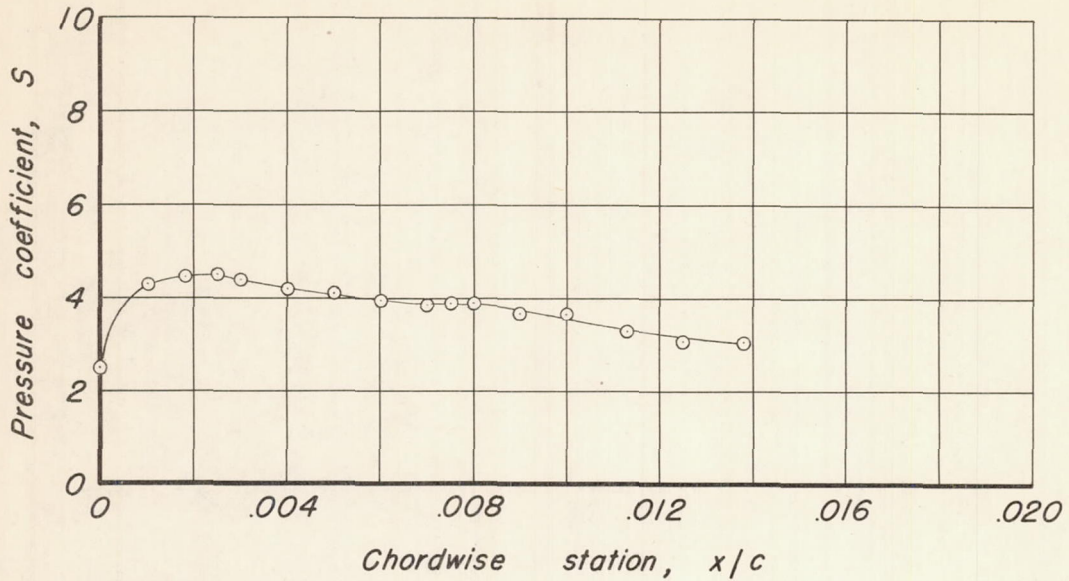
Pressure distribution



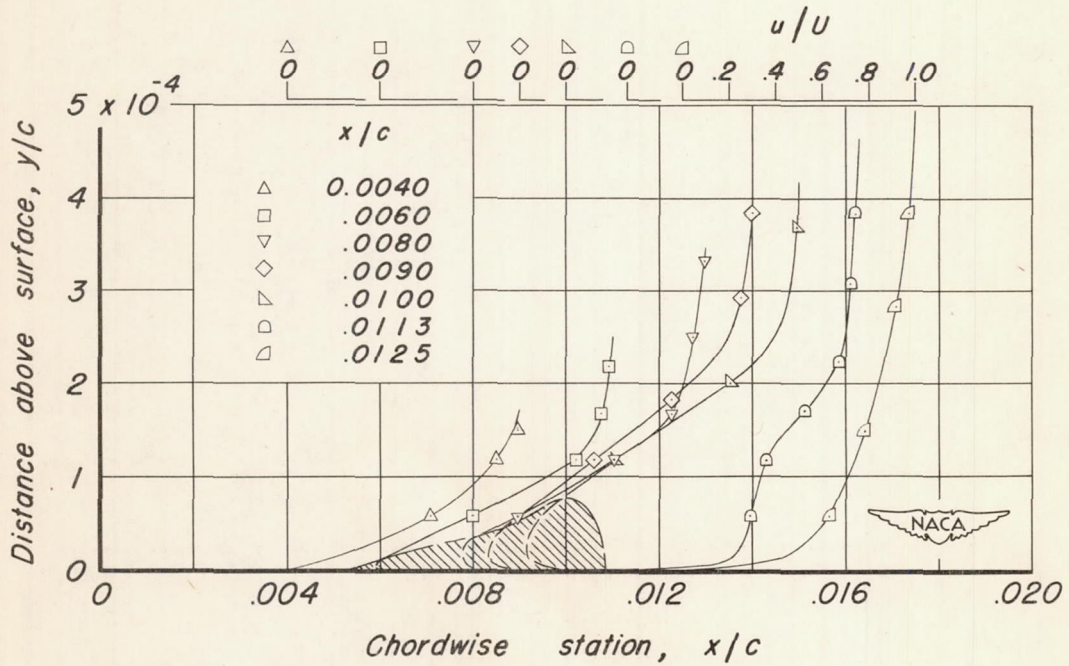
Boundary-layer velocity profiles

(a) $c_f, 0.48$; $\alpha_o, 4.0^\circ$.

Figure 7.- Pressure distributions and boundary-layer velocity profiles through the region of separated flow near the airfoil leading edge.



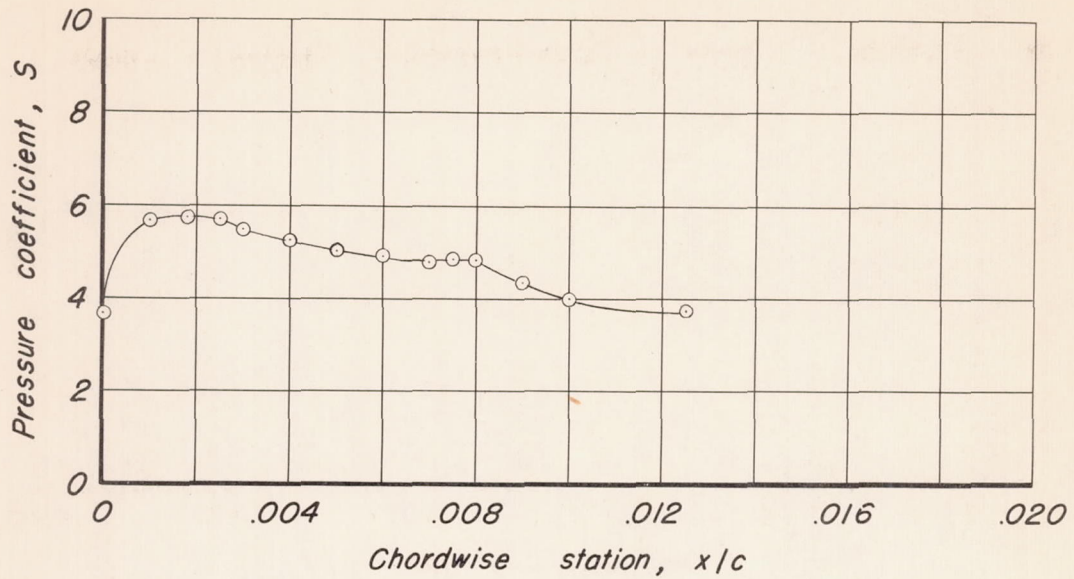
Pressure distribution



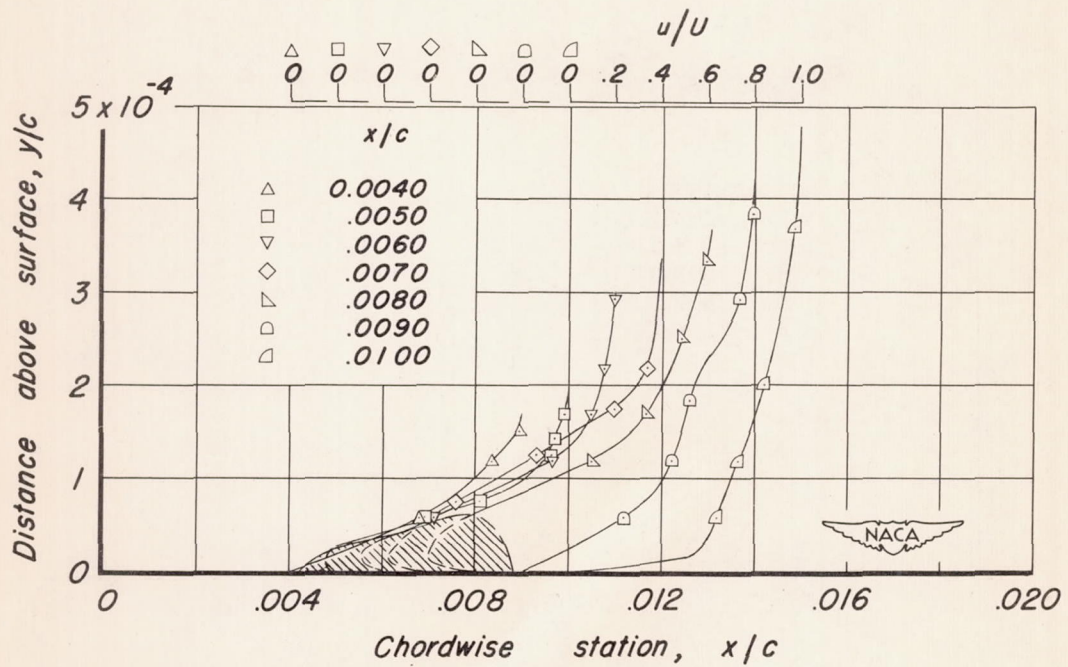
Boundary-layer velocity profiles

(b) c_l , 0.60 ; α_o , 5.0°

Figure 7 - Continued.



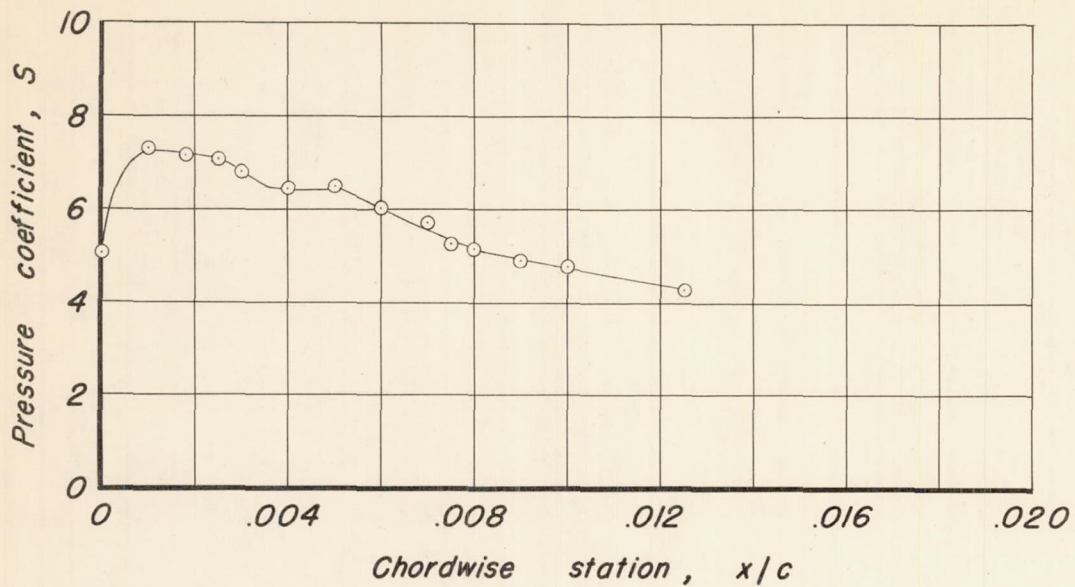
Pressure distribution



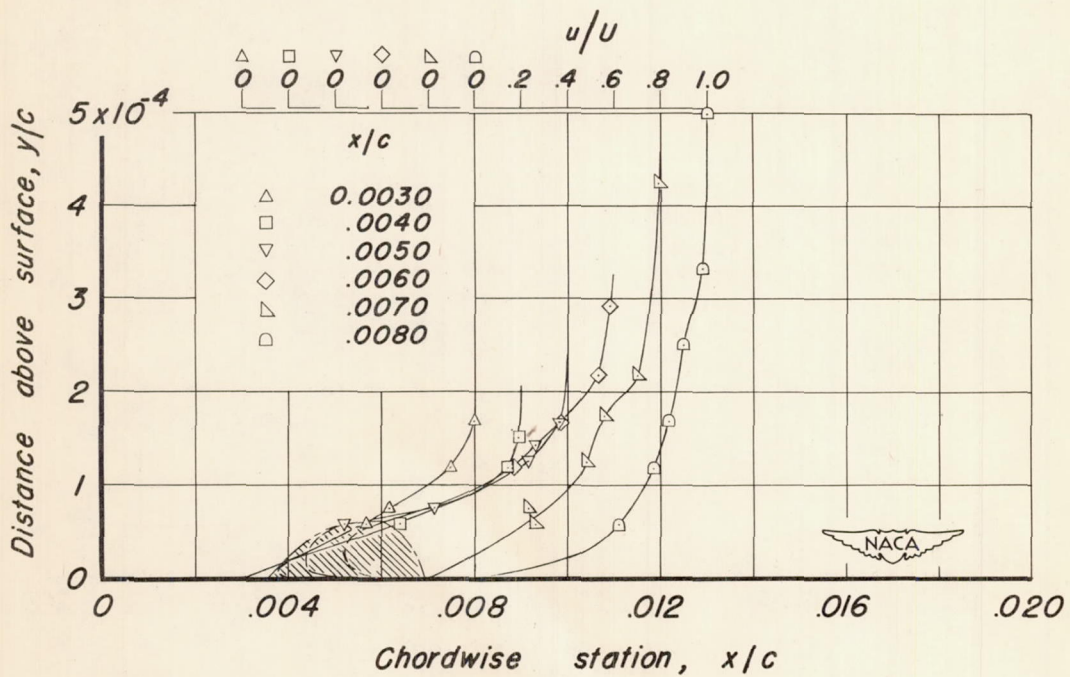
Boundary-layer velocity profiles

(c) c_l , 0.72; α_o , 6.0°.

Figure 7. - Continued.



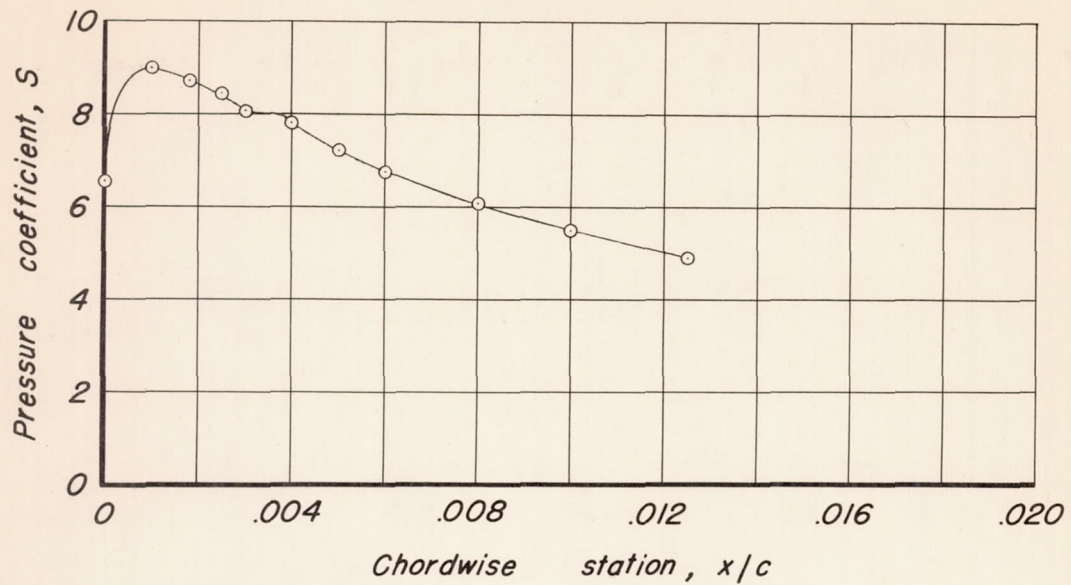
Pressure distribution



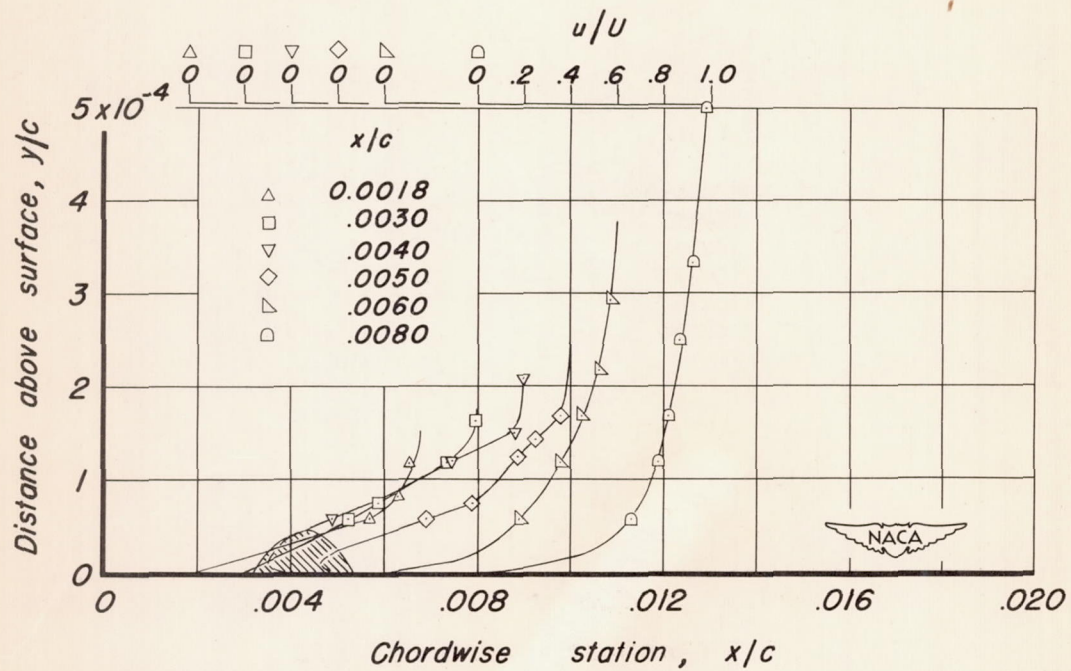
Boundary-layer velocity profiles

(d) c_l , 0.85; α_o , 7.0° .

Figure 7. - Continued.



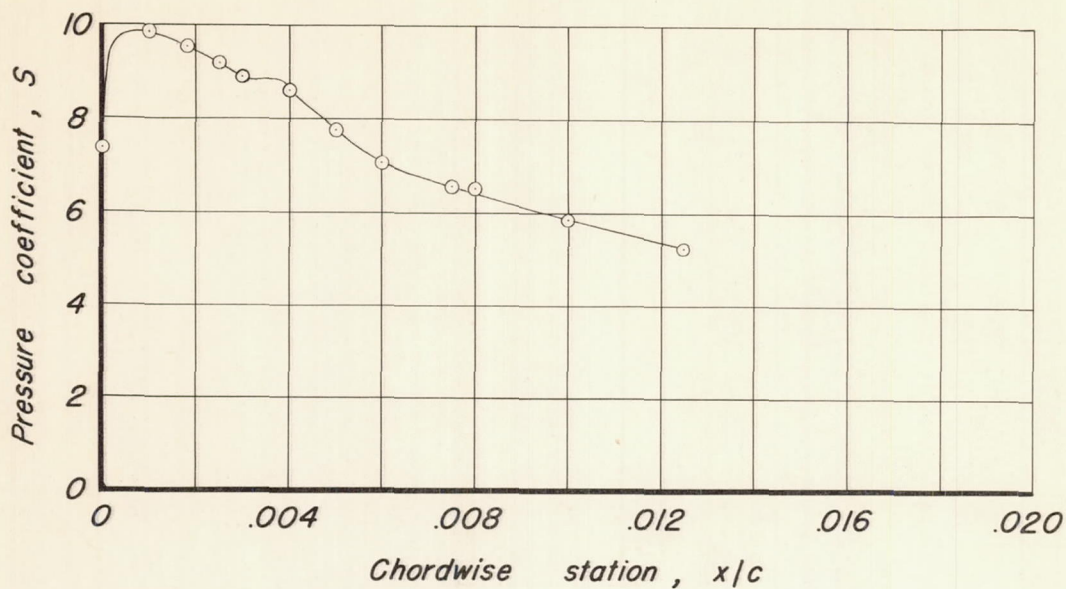
Pressure distribution



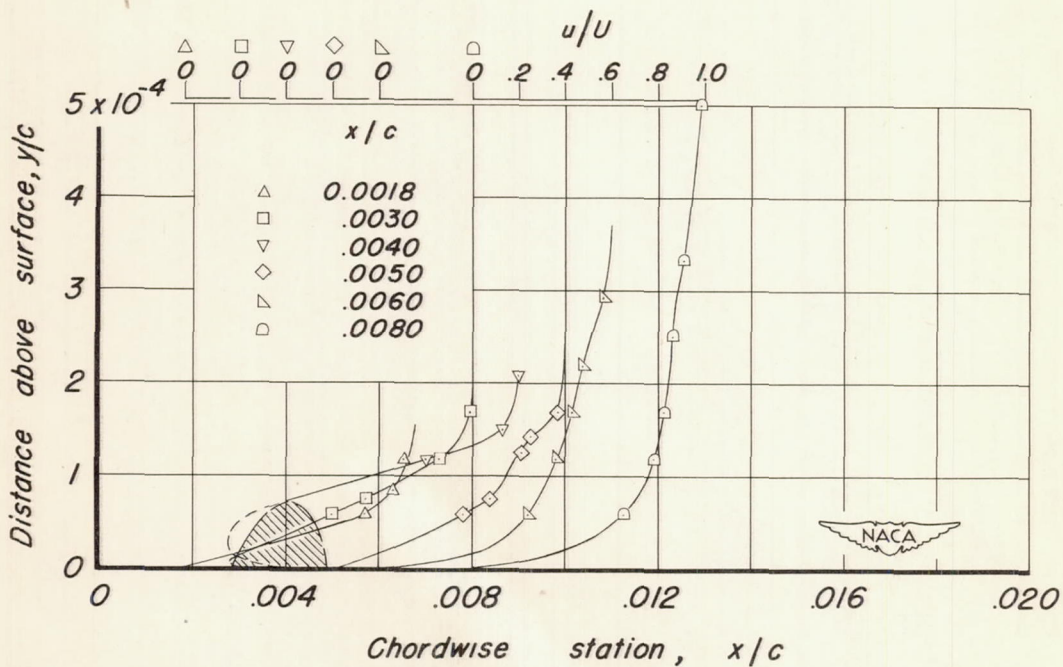
Boundary-layer velocity profiles

(e) c_l , 0.96; α_o , 8.0°.

Figure 7-Continued.



Pressure distribution



Boundary-layer velocity profiles

(f) c_l , 1.02 ; α_o , 8.5° .

Figure 7.- Concluded.

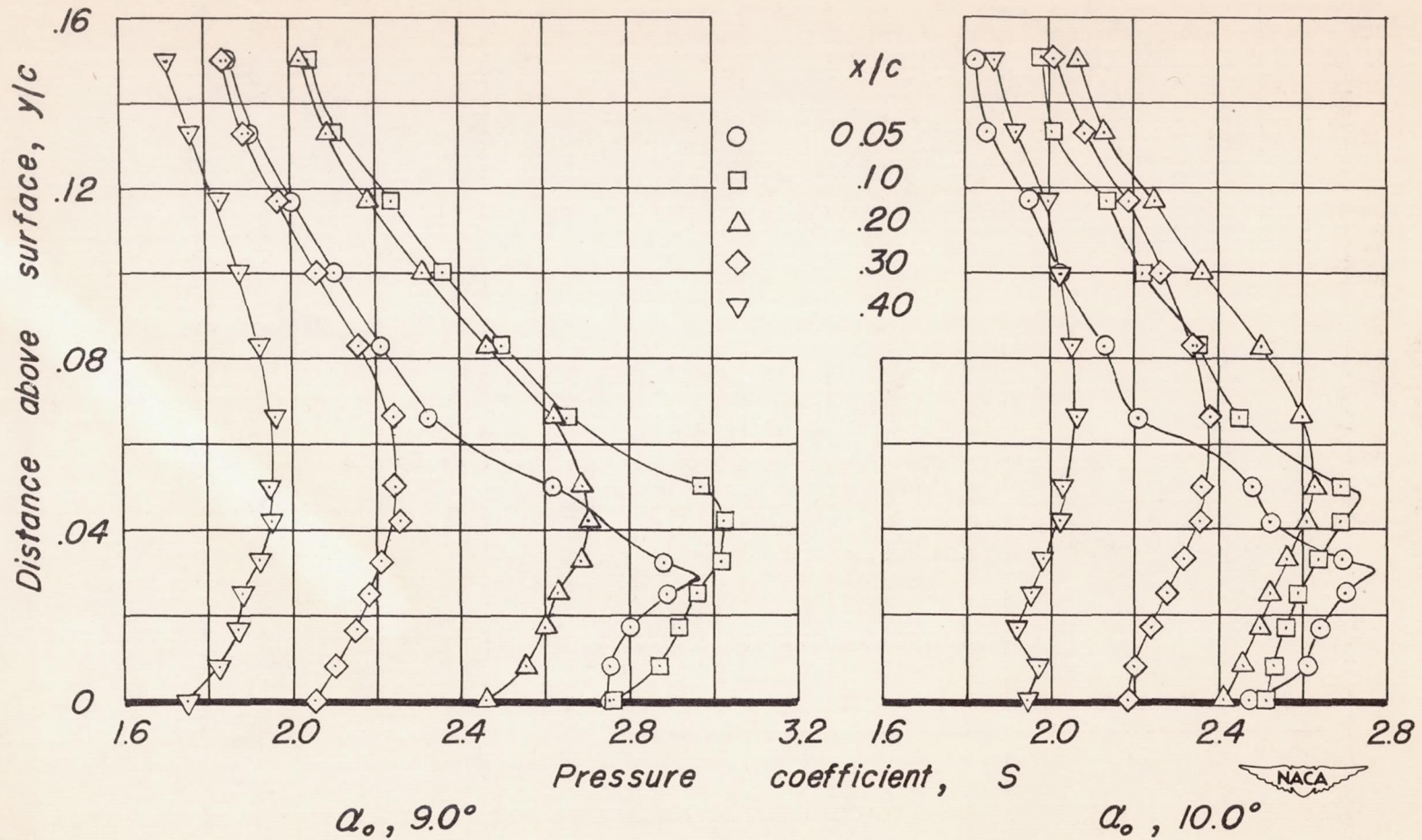


Figure 8.—Variation in the static pressure above the airfoil surface for the model in the stalled condition.

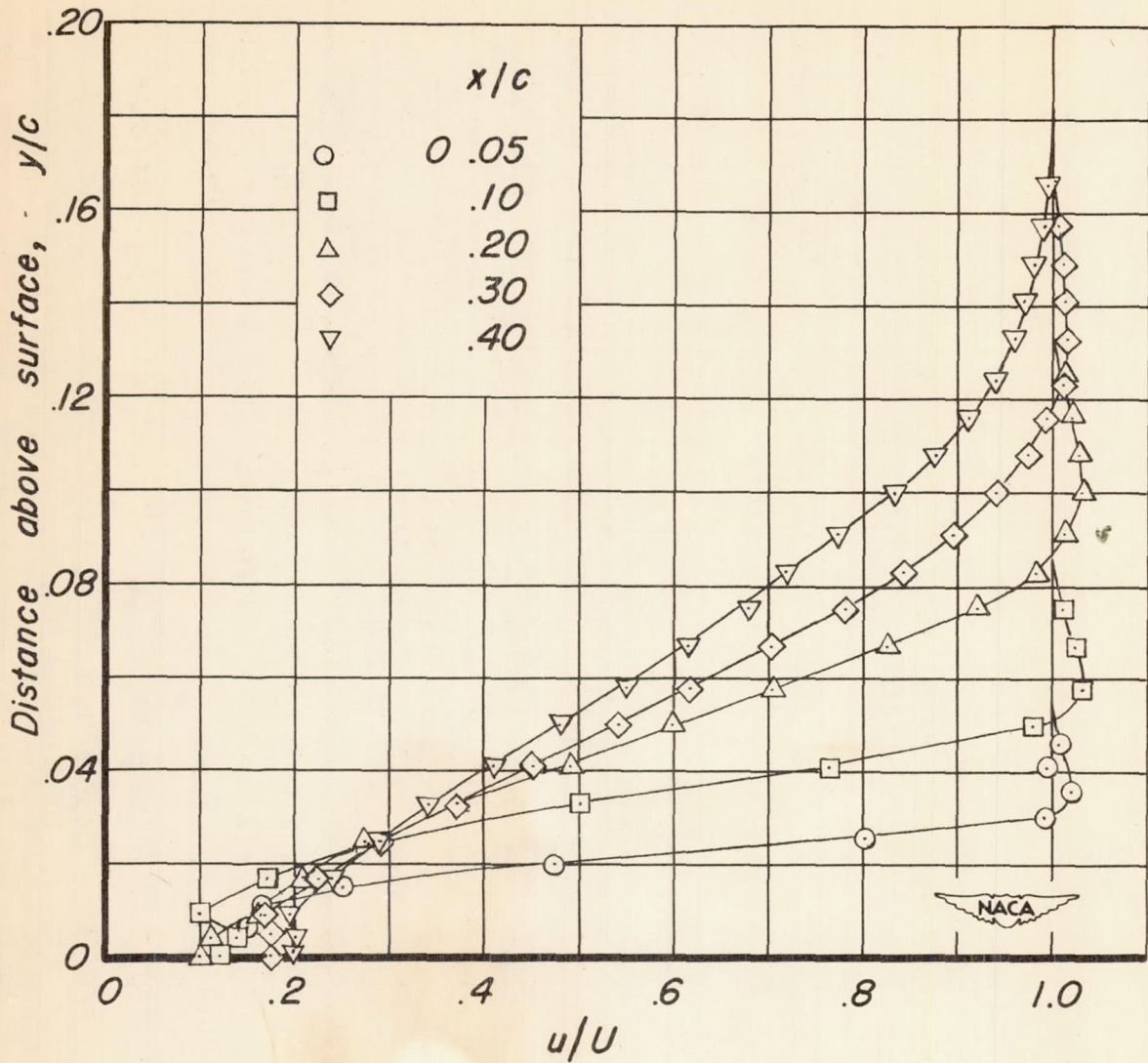


Figure 9.- Boundary-layer velocity profiles for the model in the stalled condition. $\alpha, 9.0^\circ$.